Facile Fabrication of Large-Area Atomically Thin Membranes by Direct Synthesis of Graphene with Nanoscale Porosity

Piran R. Kidambi,* Giang D. Nguyen, Sui Zhang, Qu Chen, Jing Kong, Jamie Warner, An-Ping Li, and Rohit Karnik*

Direct synthesis of graphene with well-defined nanoscale pores over large areas can transform the fabrication of nanoporous atomically thin membranes (NATMs) and greatly enhance their potential for practical applications. However, scalable bottom-up synthesis of continuous sheets of nanoporous graphene that maintain integrity over large areas has not been demonstrated. Here, it is shown that a simple reduction in temperature during chemical vapor deposition (CVD) on Cu induces in-situ formation of nanoscale defects ($\leq 2–3$ nm) in the graphene lattice, enabling direct and scalable synthesis of nanoporous monolayer graphene. By solution-casting of hierarchically porous polyether sulfone supports on the as-grown nanoporous CVD graphene, large-area (>5 cm^2) NATMs for dialysis applications are demonstrated. The synthesized NATMs show size-selective diffusive transport and effective separation of small molecules and salts from a model protein, with $\approx 2–100\times$ increase in permeance along with selectivity better than or comparable to state-of-the-art commercially available polymeric dialysis membranes. The membranes constitute the largest fully functional NATMs fabricated via bottom-up nanopore formation, and can be easily scaled up to larger sizes permitted by CVD synthesis. The results highlight synergistic benefits in blending traditional membrane casting with bottom-up pore creation during graphene CVD for advancing NATMs toward practical applications.

2D materials like graphene offer transformational opportunities for membrane-based separation technologies.[1,2] Graphene's ability to sustain nanoscale pores (via the formation of defects) in its atomically thin (≈ 0.34 nm) lattice,[3,4] coupled with high mechanical strength (when appropriately supported),[5,6] allows for the realization of nanoporous atomically thin membranes (NATMs).[1,3,7–18] Such NATMs with extremely high permeance and selectivity[3,4,7,8,12–20] are expected to offer significant advances over current state-of-the-art polymer membranes, specifically for diffusion-based separation processes such as dialysis.[9]

However, i) large-area membrane quality graphene synthesis[1,21,22] and transfer to suitable porous supports (without polymer residue or other contamination from transfer),[1,9,21,23–26] ii) mitigation of nonselective leakage by plugging tears/damages to graphene from transfer and subsequent processing during membrane fabrication,[1,9,13,26] and most importantly iii) the formation of nanopores with a high density and narrow size distribution using cost-effective, scalable processes[1,9,13,27,28] are some of the major challenges that need to be collectively addressed to realize NATMs for practical applications.[22,29] Here, we note that large-area monolayer graphene synthesis has been demonstrated via roll-to-roll chemical vapor deposition (CVD) processes.[22,30] Further, graphene transfer at large scale has also been shown[30,31] (although complete elimination of polymer residue remains nontrivial)[17,32,33] and widely used scalable membrane manufacturing techniques such as interfacial polymerization have been adapted to effectively plug leakage across tears/damage in graphene.[13] However, facile, cost-effective processes to form nanoscale defects in

Prof. P. R. Kidambi
Department of Chemical and Biomolecular Engineering
Vanderbilt University
Nashville, TN 37235-1826, USA
E-mail: piran.kidambi@vanderbilt.edu

Prof. P. R. Kidambi, Dr. S. Zhang, Prof. R. Karnik
Department of Mechanical Engineering
Massachusetts Institute of Technology
Cambridge, MA 02139, USA
E-mail: karnik@mit.edu

Dr. G. D. Nguyen, Dr. A.-P. Li
Center for Nanophase Materials Sciences
Oak Ridge National Laboratory
Oak Ridge, TN 37831, USA

Prof. S. Zhang
Department of Chemical and Biomolecular Engineering
National University of Singapore
Singapore 117582, Singapore

Dr. Q. Chen, Prof. J. Warner
Department of Materials
University of Oxford
Oxford OX1 3PH, UK

Prof. J. Kong
Department of Electrical Engineering and Computer Science
and Research Laboratory of Electronics
Massachusetts Institute of Technology
Cambridge, MA 02139, USA

**ADVANCED
SCIENCE NEWS**

www.advancedsciencenews.com

**ADVANCED
MATERIALS**

www.advmat.de

the graphene lattice, specifically with a narrow size distribution and high density over large areas remain elusive. We emphasize that size selective separations with large-area NATMs have so far been limited to using top-down approaches for nanopore formation in graphene, i.e., lithography,[3] ion bombardment followed by acid etch,[13,14,24,26] oxygen plasma etching,[9,24,27,28] ion bombardment followed by oxygen plasma etch,[34] and oxide nanoparticle induced etching,[10] among others.[35–40] Top-down approaches for nanopore formation generally add multiple processing steps, increasing process complexity for membrane fabrication and in some cases are not scalable.[3,13]

The synthesis of graphene and other 2D materials has primarily focused on applications in electronics[31,41,42] with an emphasis on minimizing defects in the lattice and/or grain boundaries,[43,44] and CVD has emerged as one of the most practical routes for scalable, cost effective, high-quality continuous monolayer 2D material synthesis.[45–47] However, the large and multidimensional parameter space for CVD (catalyst and its crystallography, pressure, temperature, gas ratio, partial pressure, etc.) makes process optimization for tailoring graphene's properties for membrane applications nontrivial.[21,45–47] While some size-selective transport across intrinsic defects in graphene has indeed been reported,[14,21,23] the ability to controllably make nanopores during synthesis by CVD over large areas for NATM applications is lacking.

Here, we show that it is indeed possible to effectively leverage the parameter space for graphene CVD and directly synthesize useful nanoporous graphene for NATM applications. A reduction in temperature during graphene CVD on Cu allows for scalable in-situ nanopore creation via the formation and/or growth of intrinsic nanoscale defects in the graphene lattice. Further, by tuning the casting of polyether sulfone (PES) to form ≈50 μm thick hierarchical porous support directly on top of the synthesized nanoporous graphene[22] we demonstrate a novel process to directly synthesize graphene-based NATMs with minimum number of processing steps for diffusion-based separation of molecules by dialysis.

The synthesized NATMs show size-selective transport, i.e., effective desalting of small model molecules (≈0.2–1.355 kDa) and proteins (≈14 kDa), with ≈2–100 × increase in permeance along with better/comparable selectivity to state-of-the-art commercial polymeric membranes (0.1–0.5, 0.5–1, 3.5–5, 8–10 kDa). The NATMs synthesized here also show ≥2 × increase in measured permeance compared to previously demonstrated nanoporous graphene membranes wherein pores were created by oxygen plasma etching.[9] To the best of our knowledge this is the first demonstration of a fully functional large area (>5 cm^2) NATM with bottom-up nanopore formation combined with a scalable, cost-effective transfer procedure to a customizable hierarchically porous polymer support for dialysis and desalting applications.

Prior studies in the literature, i.e., detailed semi-in-situ scanning tunneling microscopy (STM)[48] and our own exploration of the parameter space of graphene CVD for atomically thin membrane and barrier applications[21] identified temperature as one of the main parameters influencing the formation of intrinsic defects in CVD graphene on Cu.[45] However, the nature of these intrinsic defects formed at lower CVD process temperatures and specifically how they influence mass transport in

large area atomically thin membranes remain relatively unexplored,[14] primarily limited by the lack of a simple technique to probe nanometer sized defects/pores over large area.[23] To aid such an evaluation, we transferred CVD graphene synthesized at different process temperatures to polycarbonate track etched (PCTE) supports with well-defined, isolated cylindrical pores ≈200 nm using a polymer-free transfer process (see **Figure 1**A) that typically yields ≈70–90% coverage.[9,13,14,20,21]

Successful graphene transfer can be identified by optical imaging of graphene on PCTE (see Figure 1B) after transfer from Cu, where the dark square corresponds to graphene and the white surrounding region is the PCTE support. Scanning electron microscopy (SEM) images further confirm graphene transfer to PCTE (see Figure 1C–E) where the graphene-covered PCTE pores (≈200 nm dark circular features) appear darker due to the electrical conductivity of graphene and the un-covered PCTE pores appear brighter.[9,13,14,20,21] Additionally, large tears and other damage inevitably introduced during mechanical pressing stage of transfer (red arrows, Figure 1C,E) and wrinkles (yellow arrows, Figure 1C,D) in CVD graphene are also seen; consistent with prior reports for polymer-free graphene transfer to PCTE supports.[9,21,23]

Raman spectra were measured for CVD graphene samples synthesized at different temperatures (see **Figure 2**A) prior to transport experiments as a qualitative measure of intrinsic defects in the hexagonal graphene lattice. Raman spectra for CVD graphene synthesized at ≥1000 °C look alike, with peaks corresponding to high quality graphene,[49] i.e., 2D (≈2700 cm^{-1}), G (≈1600 cm^{-1}) peaks and a complete absence of the D peak (≈1350 cm^{-1}). A decrease in CVD process temperature however is accompanied by a clear and distinct increase in the D peak and the onset of a D' peak (≈1645 cm^{-1}), particularly for temperatures ≤950 °C indicating the presence of defects and dangling bonds in the graphene lattice.[49] The defect spacing (L_D) computed using the I_D/I_G ratios from the Raman spectra also decreases from ≈70–90 nm to ≈19–30 nm with a reduction in synthesis temperature (see Figure S1, Supporting Information).[49]

To assess the size and mass transport properties through these defects, we measured diffusive flux across the graphene + PCTE and normalized it with the diffusive flux across the bare PCTE support membrane (see Figure 2B) for solutes such as KCl (salt, hydrated K$^+$ and Cl$^-$ ions ≈0.66 nm), L-Tryptophan (amino acid, ≈0.7–0.9 nm, 204 Da), Allura Red Dye (food coloring dye, ≈1 nm, 496 Da), Vitamin B12 (vitamin, ≈1–1.5 nm, 1355 Da), and Lysozyme (egg protein, ≈3.8–4 nm, 14300 Da). We note that diffusion-driven transport across the synthesized graphene + PCTE membranes could arise from i) nonselective transport through large tears in the graphene or ii) selective transport through nanopores in the graphene.[9,23] For graphene synthesized ≈1050 °C the normalized flux

$\left(\dfrac{\text{diffusive flux graphene} + \text{PCTE}}{\text{diffusive flux across PCTE}} \right)$ for all species are similar,

indicating the absence of selective nanometer and sub-nanometer-sized defects, and that transport occurs primarily through nonselective large tears.[9,23] By contrast, a decrease in graphene CVD growth temperature leads to selective transport (Figure 2B) such that the normalized flux of KCl > L-Tryptophan (L-Tr) > Allura Red (Allura) > Vitamin B12 (B12), which
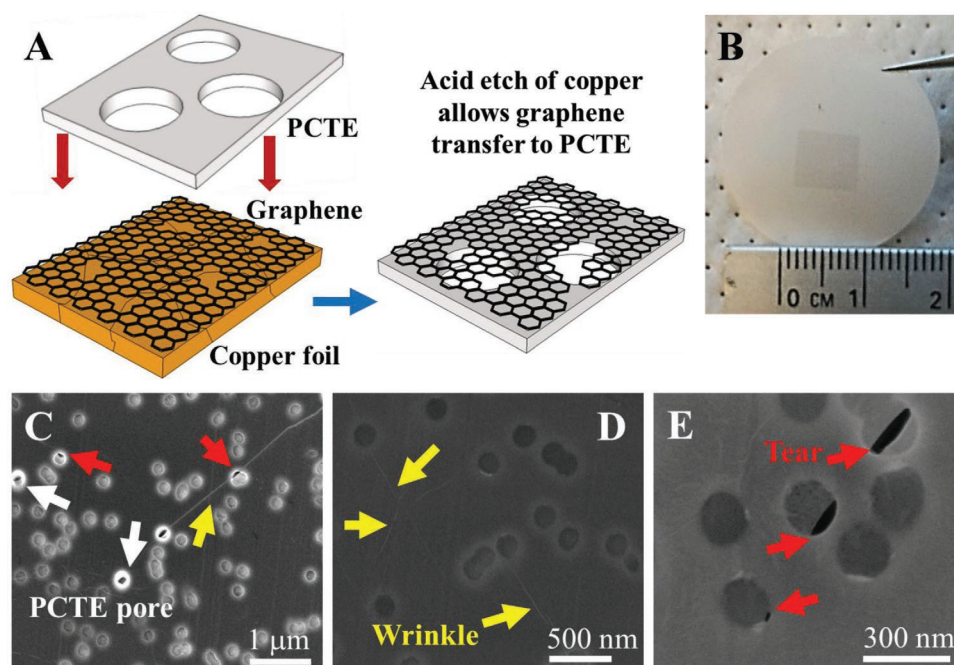
Figure 1. Polymer-free graphene transfer to polycarbonate track etched (PCTE) supports. A) Schematic of graphene transfer process to polycarbonate track etched (PCTE) supports with 200 nm pores. Nanoporous graphene on copper foil is mechanically pressed against PCTE followed by etching of copper. B) Optical image of graphene on PCTE support. The black square in the image is graphene. C–E) Scanning electron microscopy (SEM) images of graphene on PCTE support. Red arrows indicate tears inevitably introduced during the mechanical pressing during transfer, yellow arrows show wrinkles in the graphene film and white arrows show open PCTE pores ≈200 nm without graphene.

suggests the presence of nanometer and sub-nanometer sized defects in addition to nonselective flow across large tears.[9,21,23] The graphene synthesized at 900 °C shows maximum separation between normalized fluxes of KCl and L-Tryptophan, while the graphene synthesized at 850 °C shows similar trends albeit with slightly lower normalized flux difference between KCl and L-Tryptophan. Such preferential transport of KCl compared to L-Tryptophan is indicative of the presence of sub-nanometer to nanometer sized defects ≤2 nm.[23]

High-resolution transmission electron microscopy images of the graphene synthesized at 900 °C transferred to holey Si_3N_4 grids indeed confirms the presence of nanometer-sized (≈2–3 nm) defects in the graphene lattice (see Figure 2C–F, red arrows) in agreement with transport measurements (Figure 2B) and Raman spectra (Figure 2A). We note the transfer process to rigid Si_3N_4 grids used a polymer carrier layer that typically leaves residue on the graphene surface (see Figure S2, Supporting Information) making imaging nontrivial, since such polymer residues typically adhere to defects (covers defects) in the graphene lattice.[50] STM images (Figure 2G–I) acquired directly on graphene (synthesized at 900 °C) on the Cu foil also show the presence of nanometer sized defects in the graphene lattice. We note that the defects observed in STM are smaller and their density is higher than those observed in TEM. These observations could potentially be attributed to polymer residue adhering to defects in the graphene during TEM sample preparation. Further we note that heating in vacuum of graphene on Cu for STM measurements for reducing copper oxide at the graphene/Cu interface[46,51] could in principle introduce additional defects. However, graphene on Cu stored in a

vacuum desiccator for ≈8 months did not show major differences in defect density compared to graphene on Cu stored for ≈15 months, even though more oxidation of Cu is expected for the latter. Taken together, a simple reduction in the graphene CVD temperature allows for in-situ nanopore creation in the graphene lattice in a scalable, cost-effective, single-step process in direct contrast to current top-down methods of nanopore creation.[1,9,13,27,28]

We note the defects observed here could have formed during the different stages of the CVD process, e.g., defects could form during growth: a) directly within the individual domains that make up the continuous polycrystalline graphene film,[48,52–54] b) due to incomplete merging of domain boundaries,[55–57] c) via etching of graphene either during synthesis or while cooling the graphene on Cu foil in the growth mixture, specifically at temperatures where the CH_4 can no longer dissociate to supply carbon but H_2 or other impurities can etch the synthesized graphene.[21,45] Hence, it is possible that the defects may be specific to the synthesis conditions used and/or CVD system-specific leakages of air and/or other contaminants.[45–47] However, we emphasize that similar effects have been observed with commercially available graphene (Figure 2B) and other prior studies.[14] Further, the defects formed during CVD could also have been potentially enlarged by oxidation of Cu underneath the graphene during storage.[46,51] However, we tested graphene stored for ≈15 days and ≈1 year and found no major differences. Further, we note that in prior studies graphene synthesized at 1050 °C and stored for up to 6–12 months also did not show selective transport indicating that defect formation due to oxidation of the Cu foil underneath is negligible.[21]
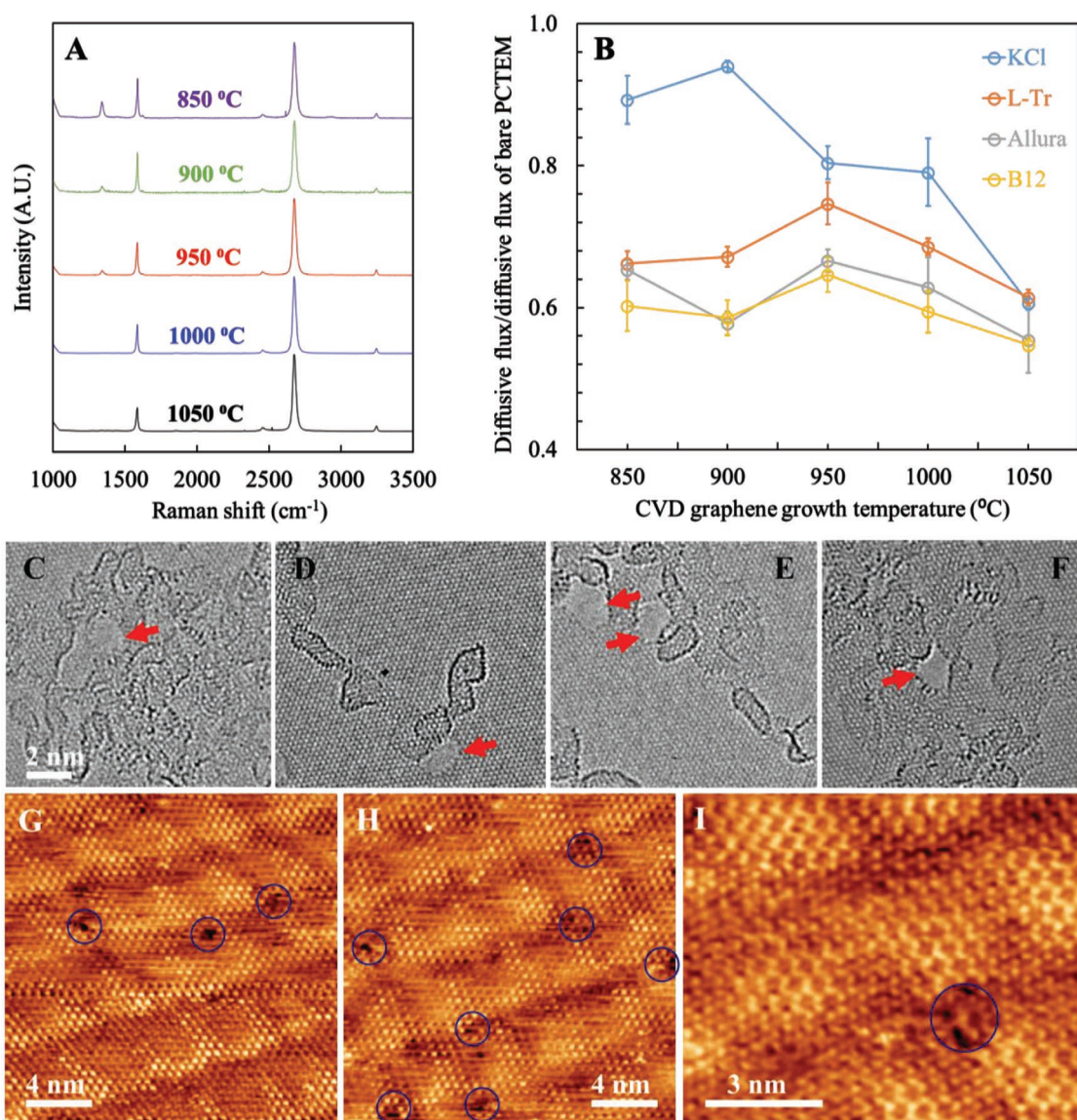
Figure 2. Assessment and characterization of nanometer-scale defects in CVD graphene. A) Raman spectra for monolayer graphene synthesized at different temperatures by chemical vapor deposition (CVD) after transfer to 300 nm SiO_2/Si wafer. The emergence of the D peak at lower synthesis temperatures is indicative of defects in the hexagonal graphene lattice. B) Diffusive transport across CVD graphene transferred on to PCTE membrane supports normalized by transport across bare PCTE support indicates preferential transport of KCl ≈0.66 nm compared to L-Tryptophan (L-Tr, ≈0.7–0.9 nm), Allura red dye (Allura, ≈1 nm), and Vitamin B12 (B12, ≈1–1.5 nm). Such diffusive transport is indicative of sub-nanometer to nanometer sized defects in graphene.[9,21,23] Note the 1000 °C data points in B correspond to commercially available graphene from Graphenea. C–F) High-resolution transmission electron microscopy images of the graphene synthesized at 900 °C show the presence of nanometer sized defects/holes (marked by red arrows). G–I) Atomic resolution STM images acquired at different locations of the graphene on Cu foil synthesized via CVD at 900 °C show the presence of nanometer sized defects/holes (marked by blue circles).

However, we note that most of the pores observed by TEM or STM occur within crystal domains and not at grain boundaries, which suggests that grain boundary-independent mechanisms, such as the formation of a point defect within a crystal domain and its growth, are responsible for the created pores.[48,52–54] Further elucidation of the precise atomistic mechanism of the formation of such defects is a topic of future research requiring nontrivial in-situ STM[48] on polycrystalline Cu at temperatures where the Cu surface is extremely mobile[46] and well beyond the scope of the current study.

Having established a facile process for bottom-up synthesis of nanoporous graphene, we focus on developing processing routes to realize large area monolayer nanoporous graphene suspended on suitable porous supports in a clean, cost-effective and scalable manner (see **Figure 3**A). Our approach consists of blending technological know-how in traditional membrane processing, i.e., polymer casting with the synthesized nanoporous CVD graphene (Figure 3A). Polymer casting for the synthesis of conventional desalination membranes is a scalable and well-developed manufacturing technology[58,59] and PES support
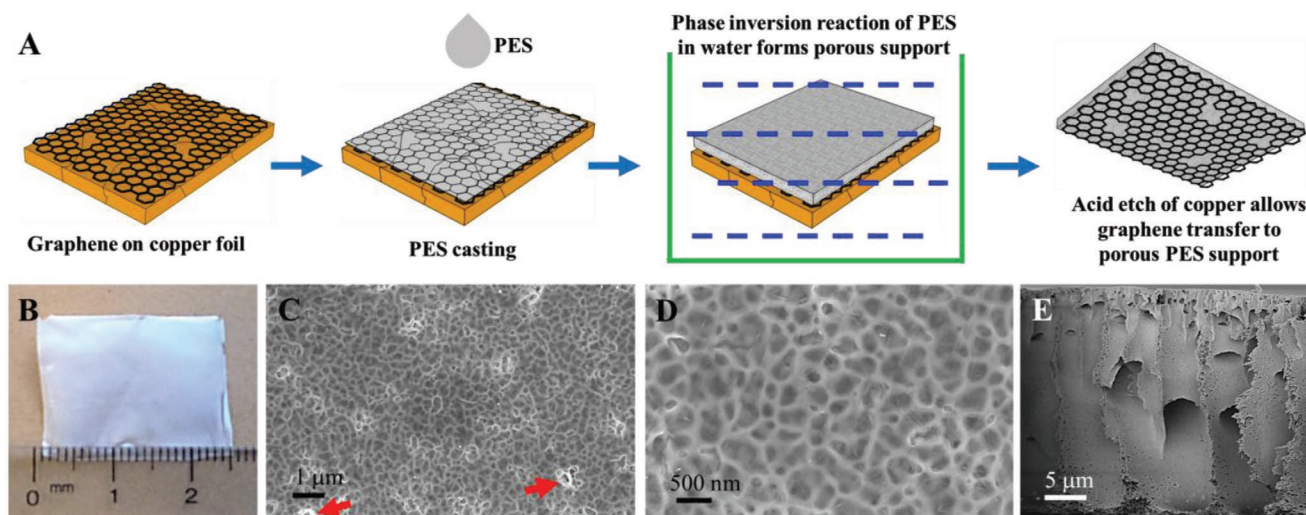
**ADVANCED
SCIENCE NEWS**

www.advancedsciencenews.com

**ADVANCED
MATERIALS**

www.advmat.de

Figure 3. Polymer casting on nanoporous CVD graphene for facile NATM fabrication. A) Schematic of nanoporous graphene transfer to micro/macroporous polyethersulfone (PES) support membrane. B) Optical image of large-area graphene transferred to PES support. C,D) SEM images of graphene on porous PES supports. E) Cross section of PES support shows a hierarchical pore structure with ≈200–500 nm pores near the top (underneath graphene) which connect to much larger pores approximately several µm further below. The pore structure also has micropores that connect laterally throughout the PES support.

membranes for pressure-driven separations with graphene have been recently demonstrated.[26]

By tuning the composition of the casting solution, the thickness of the casting film and controlling the time for phase inversion we realize large-area graphene NATMs with hierarchically porous PES supports that offer low resistance to diffusion-driven transport while simultaneously supporting nanoporous graphene effectively (Figure 3A).[22] Optical images show large-area nanoporous graphene (>5 cm²) on PES supports (Figure 3B) and SEM images (Figure 3C,D) shows graphene (identified by the wrinkles) suspended on porous PES supports with features ≈100–500 nm.[22] While the vast majority of PES pores are indeed covered by graphene, the graphene on some PES pores shows signs of damage from processing in the form of small tears (red arrows in Figure 3C). SEM images of the cross section of graphene + PES (Figure 3E) shows an interesting morphology for the PES supports. The PES supports shows a hierarchical pore structure with ≈200–500 nm pores near the top (directly underneath graphene, consistent with Figure 3C,D) which connect to much larger pores approximately several µm further below.[22] Further, the pore structure also has micro-pores that connect laterally throughout the PES support.[22] Such a pore structure is ideal to facilitate the divergent demands of low resistance to diffusion-driven transport while simultaneously supporting nanoporous graphene effectively and allows for facile fabrication of graphene NATMs.[22]

In conventional dialysis, a relatively thick semi-permeable polymer membrane with tortuous pores separates a sample solution from a dilute receiving solution.[9] The concentration gradient across the membrane induces selective diffusion of molecules below the membrane pore size (cutoff) into the receiving solution while larger molecules are retained inducing separation.[9,60] The simplicity, gentle processing conditions, and low energy requirements for dialysis have resulted in its widespread use in bioprocessing to separate small molecules from larger molecules, e.g., salts, dyes, reducing agents from

proteins, DNA, RNA; in buffer exchange processes, peptide purification and/or removal of residual reactants.[9,60] The rate of diffusion across dialysis membranes is given by

$$J = P \times \Delta c = \frac{D}{L_{eff}} \times \Delta c \tag{1}$$

where, J is diffusive flux (kg m⁻² s⁻¹), P is the diffusive permeance (m s⁻¹), Δc is the solute concentration difference across the membrane (kg m⁻³), D is diffusivity of the molecule in free solution, and L_{eff} is the effective thickness of the membrane (L_{eff} also accounts for porosity and tortuosity of pores).[1,9] NATMs allow for the realization of the ultimate physical reduction in L_{eff} thereby enabling faster diffusion.[1,9] In addition to faster diffusion, the ratio of permeance of the molecules to be separated (selectivity) is also an important criteria for evaluating dialysis membrane performance.[1,9] In conventional membranes permeance increase often comes at the expense of selectivity;[1,3,4,61] however, NATMs could potentially enable higher permeances with very high selectivity as discussed below.[9]

The performance of the synthesized NATMs was evaluated using diffusion-driven transport for solutes such as KCl, L-Tryptophan, Vitamin B12, and Lysozyme (Lz) (see **Figure 4**A,B) and compared with commercially available state-of-the-art conventional polymeric dialysis membranes (0.1–0.5, 0.5–1, 3.5–5, 8–10 kDa).[9] The synthesized NATMs show distinctly higher permeance (≈2–100× increase, see Figure 4A) along with better or at the very least comparable selectivity (see Figure 4B,C, and Figure S3, Supporting Information) to conventional polymeric membranes.[9] The upper bound of ≈100× permeance increase is computed by comparing KCl permeance for Graphene + PES of ≈5.27 × 10⁻⁶ ms⁻¹ and 0.5–1 kDa commercial membrane of ≈5.40 × 10⁻⁸ ms⁻¹ and Vitamin B12 permeance for Graphene + PES of ≈7.25 × 10⁻⁷ ms⁻¹ and 0.5–1 kDa commercial membrane of ≈6.47 × 10⁻⁹ ms⁻¹, respectively. To confirm that the observed performance here arises from nanoporous graphene, we

ADVANCED
SCIENCE NEWS
www.advancedsciencenews.com

ADVANCED
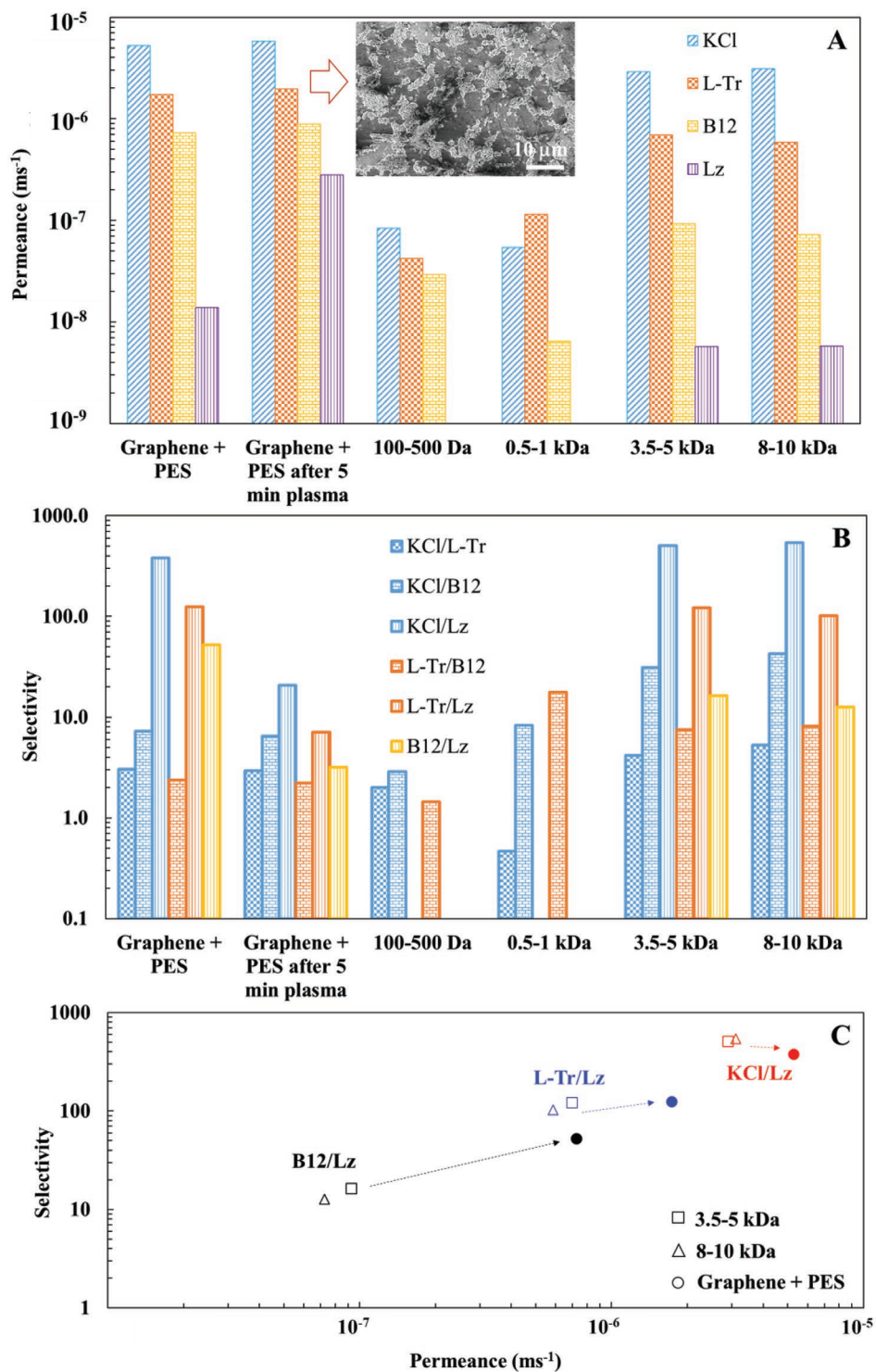MATERIALS
www.advmat.de

Figure 4. Permeance and selectivity of NATMs compared to state-of-the-art polymeric dialysis membranes. A) Diffusive permeance and B) selectivity (ratio of permeance) for KCl, L-Tryptophan (L-Tr), Vitamin B12 (B12), and Lysozyme (Lz) for commercially available dialysis membranes (adapted from ref. [9]), graphene + PES membrane before and after damage by 5 min of air plasma to destroy the graphene as seen in the SEM image in the inset in (A). C) Selectivity versus permeance for KCl/Lz (red, plotted with permeance of KCl), L-Tr/Lz (blue, plotted with permeance of L-Tr), and B12/Lz (black, plotted with permeance of B12) for graphene + PES (circles) and commercially available dialysis membranes 3.5–5 kDa (square) and 8–10 kDa (triangles).[9] Arrows are a guide for the eye to highlight improvement with graphene NATMs. Also, see Figure S2C,E,F (Supporting Information) for individual plots of selectivity versus permeance.
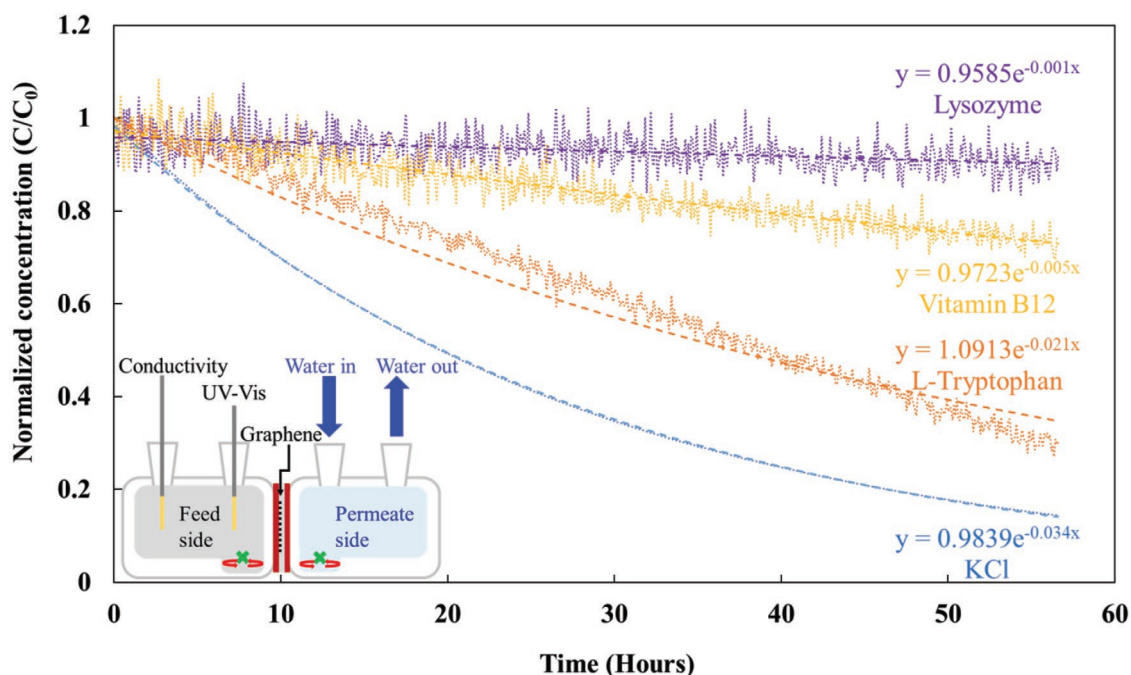
Figure 5. Size-selective separation using NATMs. Demonstration of protein (Lysozyme) de-salting and small molecule separation (KCl, L-Tryptophan, Vitamin B12) using the nanoporous graphene on PES support. Inset shows the set-up used for separation experiments.[9] Dashed lines show exponential fits to concentration profiles.

subjected the graphene + PES membrane to 5 min of air plasma which effectively destroys the graphene (see SEM inset in Figure 4A). Such damage to graphene is accompanied by more than 1.5 orders of magnitude increase in Lysozyme permeance (see Figure 4A) and explicitly clarifies the role of nanoporous graphene in the observed size-selective transport of the synthesized graphene NATMs. Interestingly, the permeance of the salt and small molecules does not change significantly after 5 min of plasma treatment (Figure 4A), indicating that the nanoporous graphene is essentially transparent for all species except lysozyme, and that the permeance is governed by the support. Therefore, further improvements are expected with thinner support layers. These observations are consistent with the presence of ≤2–3 nm pores in graphene as observed by TEM and STM (Figure 2).

The selectivity versus permeance plots (see Figure 4C) for KCl/Lysozyme (red, plotted with permeance of KCl), L-Tryptophan/Lysozyme (blue, plotted with permeance of L-Tryptophan), and Vitamin B12/Lysozyme (black, plotted with permeance of Vitamin B12) for graphene + PES (circles) and commercial dialysis membranes 3.5–5 kDa (square) and 8–10 kDa (triangles) show that our NATMs offer significant advances over conventional state-of-the-art polymeric membranes with higher permeance and good selectivity for desalting KCl/Lz and dialysis applications, notably for small molecule separation such as L-Tr/Lz and B12/Lz (also see Figure S3C,E,F, respectively, in the Supporting Information).

Finally, we demonstrate desalting of a small protein (Lysozyme, Lz) and size-selective separation of small molecules from Lz (dialysis) using the synthesized graphene NATMs (see **Figure 5**). For these separation experiments the decrease in concentration of 7 mL solutions with ≈6–7.5 × 10^{-5} M solute concentration (L-Tryptophan, Vitamin B-12, or Lysozyme, only one solute is measured in each experiment) in 0.25 M KCl on the feed side is monitored while the permeate side is constantly flushed with de-ionized water recirculated from a ≈70 L reservoir using a peristaltic pump. In all cases a decrease in concentration for both KCl and the solute is observed to follow an exponential decay consistent with the transport rate being proportional to the concentration difference (Figure 5). The rate of change of the normalized concentration of KCl (≈0.66 nm) > L-Tryptophan (≈0.7–0.9 nm) > Vitamin B12 (≈1–1.5 nm) > Lysozyme (≈3.8–4 nm) indicates size-selective transport across our NATMs (see Figure 5) consistent with observations in Figures 2B and 4A. The separation experiment indeed shows effective desalting of even small proteins such as Lysozyme- and dialysis-based small molecule separation (L-Tryptophan, Vitamin B12) from a small protein. These observations indicate that the majority of the pores in the NATMs are ≤2–3 nm, while some leakage of Lysozyme could be attributed to damage during membrane fabrication (Figure 3C). Lastly, we emphasize that our NATMs show ≥2 × increase in measured permeance compared to previously demonstrated state-of-the-art large area (cm^2) graphene membranes with pores created by oxygen plasma etching.[9]

In conclusion, we have demonstrated a novel method for facile, cost-effective, scalable synthesis of large area (>5 cm^2) NATMs by blending traditional membrane processing with novel approaches for graphene CVD on Cu. A simple reduction in the graphene CVD temperature allows for in-situ nanopore creation in the graphene lattice via the formation and growth of intrinsic nanoscale defects. Optimization of traditional membrane casting approaches to form ≈50 µm thick hierarchical porous PES support layer directly on nanoporous monolayer graphene

**ADVANCED
SCIENCE NEWS**

www.advancedsciencenews.com

**ADVANCED
MATERIALS**

www.advmat.de

allows for successful realization of graphene NATMs.[22] The NATMs show size-selective transport and effective desalting of small molecules (≈0.2–1.355 kDa) and proteins (≈14 kDa), with ≈2–100 × increase in permeance along with better/comparable selectivity to state-of-the-art commercial polymeric membranes (0.1–0.5, 0.5–1, 3.5–5, 8–10 kDa).[9] Our NATMs indeed show ≥2 × increase in measured permeance compared to previously demonstrated state-of-the-art large area (cm²) graphene NATMs.[9] Such advances in NATMs are expected to offer transformative advances in dialysis applications to separate small molecules like salts, dyes, reducing agents from larger molecules such as proteins, DNA, RNA, in processes such as buffer exchange, peptide purification, therapeutics, nano-bio separations and removal of residual reactants.[9]

Experimental Section

Graphene Growth: Graphene growth was performed in a hot-walled tube furnace as reported in detail elsewhere.[21,45,46] Cu foil (purity 99.9%, thickness 18 µm, JX Holding HA) was cleaned by sonicating it in 15% HNO₃ to remove oxides and other contaminants from the surface. It was subsequently washed with deionized water and dried in nitrogen before being annealed at 1050 °C for 60 min in 60 sccm H₂ at ≈1.14 Torr. After annealing the foil was cooled to growth temperature in 15 min and graphene growth was performed by adding CH₄ (3.5 sccm ≈2.7 Torr) to H₂ at 800–1050 °C for 30 min followed by 30 min of 7 sccm CH₄ (≈3.6 Torr) and 60 sccm H₂. The foil was rapidly cooled in the growth atmosphere at the end of the growth. Graphene on Cu used in this study was stored for anywhere from 0.5 to 15 months in desiccators in vacuum before transfer to substrates. Additionally, we also used commercially available graphene from Graphenea typically synthesized at ≈1000 °C.

Graphene Transfer: Polymer-free graphene transfers to polycarbonate track etched (PCTE) supports (≈10% porosity, 10 µm thick, non-PVP coated, hydrophobic, 200 nm cylindrical pores, Sterlitech Inc.) were performed as described elsewhere.[9,14,21] A short pre-etch in ammonium persulfate (APS-100, Transene) for 5 min was initially used to remove the graphene on Cu foil surface in contact with the quartz tube. Subsequently, the graphene on the other side was mechanically contacted with PCTE supports and the Cu foil was completely etched in APS-100. The graphene + PCTE stack was rinsed with deionized water followed by ethanol and dried at room temperature.[13,14,20]

For transfer to TEM grids a poly(methyl methacrylate) (PMMA) scaffold layer was used while the Cu was etched using ammonium persulfate (APS, 0.2 mol L⁻¹). Then the graphene/PMMA thin film was transferred onto holey Si₃N₄ TEM grids (Agar Scientific AG21580) and PMMA was removed using acetone at room temperature. Additional cleaning using elevated temperatures was not performed to minimize inadvertent introduction of additional defects. Similar methods were also used for graphene transfer to 300 nm SiO₂/Si wafer for Raman spectroscopy.

Hierarchically Porous Support Casting: Casting polymer solution was prepared by mixing ≈16 wt% PES resin, ≈82 wt% N-methyl-2-pyrrolidone, and ≈2 wt% isopropanol, and baked in an oven at 75 °C for ≈24 h and subsequently allowed to cool and degas for ≈12 h.[22] The casting was performed after sticking all the edges of graphene on Cu foil (pre-etched in APS-100 for 5 min to remove the graphene on the back side) to an aluminum plate with Scotch tape (magic tape 810 19 mm width, ≈50 µm thickness).[22] A disposable culture tube (diameter 13 mm, height 100 mm) with three windings of Scotch tape was used to spread the PES solution on graphene on Cu in one, swift unidirectional stroke.[22] The PES + graphene + Cu stack was immersed in a deionized water bath for 30 min after which the stack was released from the aluminum plate and the Cu foil was etched in APS-100 to leave graphene suspended on a hierarchically porous PES support.[22]

The graphene + PES stack was rinsed with deionized water followed by ethanol and dried at room temperature.[22]

Characterization: SEM images were obtained using a Helios Nanolab Dualbeam 600 (2 kV, 86 pA, 4 mm working distance using immersion mode with an Everhart-Thornley detector) or Zeiss Supra/Ultra/Ultra Plus (2 kV, 4–6 mm working distance using an InLens detector). A Horiba Raman spectrometer with a 532 nm source was used for Raman spectroscopy. TEM images were acquired using a JEOL JEM-2200MCO TEM operated at 80 kV with a CEOS imaging aberration corrector. The images were processed using a fast Fourier transform (FFT) band pass between 100 and 1 pixels, followed by a 2 pixel Gaussian blur and adjusted for brightness and contrast. STM images were acquired using an ultrahigh vacuum STM at room temperature. Graphene on Cu was annealed at ≈380 °C in UHV for 16 h prior to measurements at setting point of 0.5 V and 0.5 nA. A Harrick Plasma cleaner PDC-001 (maximum power 30 W, 500 mTorr air) was used to damage graphene on PES.

Transport Measurements: Transport measurements were performed as described in previous work,[9,13,21–23] as follows. Graphene + PCTE/PES stack was sandwiched between two side-by-side diffusion cells (Permegear Inc., 5 mm orifice, 7 mL volume) for diffusion-driven flow measurements.[9,21–23] The graphene + PCTE/PES stack was first rinsed with ethanol (KOPTEC 200 proof ethanol anhydrous) to ensure wetting of all pores.[9,21–23] After ethanol, the graphene + PCTE/PES stack was rinsed with deionized water for five times.[9,21–23] All measurements were performed in triplicates.

Diffusion-driven transport of KCl was measured using 0.5 M KCl in deionized water in the feed side (solution in direct contact with graphene) diffusion cell while the increase in conductivity of deionized water on the permeate side was measured with the help of a conductivity meter (eDAQ-Isopod or Mettler Toledo S230).[9,13,21–23] The slope of concentration as a function of time after steady state was established (i.e., 600–900 s) was used to calculate normalized flux for KCl $\left(\dfrac{\text{diffusive flux across graphene} + \text{PCTE}}{\text{diffusive flux across PCTE}} \right)$.[9,13,21–23] However, diffusion-driven transport of Allura Red AC (98%, Sigma-Aldrich), L-Tryptophan (99%, Alfa Aesar), Vitamin B12 (Cyanocobalamin > 98%, Alfa Aesar), and Lysozyme (ultrapure grade, VWR International) were measured using a mixture of 1 × 10⁻³ M of each solute molecule in 0.5 M KCl on the feed side while measuring their diffusion into 0.5 M KCl on the permeate side with a UV–vis spectrometer (Agilent – Cary 60).[9,13,21–23] The difference in absorbance compared to the reference for deionized water (710 nm), Allura Red (510 nm), L-Tryptophan (279 nm), Vitamin B12 (360 nm), and Lysozyme (282 nm) were used to compute concentrations from UV–vis spectra, respectively.[9,13,21–23] Vigorous stirring was ensured in both cells to minimize concentration polarization effects and the ratio of the slope of concentration increase as a function of time for graphene + PCTE to PCTE was used to compute the normalized flux $\left(\dfrac{\text{diffusive flux across graphene} + \text{PCTE}}{\text{diffusive flux across PCTE}} \right)$.[9,13,21–23]

Permeance was computed using $\left(\dfrac{V \times \frac{dC}{dt}}{\Delta C \times A} \right)$ where V is volume of the diffusion cell, A is the area of membrane measured in the diffusion cell (5 mm orifice diameter), and ΔC is the concentration difference between the solutes in the solution in both cells.[9,13,21–23] The ratio of permeance between the diffusing species was used to calculate selectivity.[9,13,21–23]

For separation experiments conductivity and UV–vis spectra were measured on the feed side and the permeate side (see inset in Figure 5) was continuously flushed with de-ionized water re-circulated from a reservoir (volume of ≈70L) using a peristaltic pump and an over flow arrangement to return the spill over water to the reservoir.[9,13,21–23]

Commercial dialysis membranes 100–500 Da (Spectrum lab CE Spectra Por), 500–1000 Da (Spectrum lab CE Spectra Por), 3500–5000 Da (Spectrum lab Spectra Por, dry biotech regenerated cellulose), and 8000–10000 Da (Spectrum lab CE Spectra Por, dry biotech regenerated cellulose) were measured for comparison.[9,13,21–23] The time for contact with ethanol during initial membranes mounting and rinsing was minimized to ≈5 min for commercial membranes.[9,13,21–23]

Supporting Information

Supporting Information is available from the Wiley Online Library or from the author.

Acknowledgements

Conflict of Interest

The authors declare no conflict of interest.

Keywords

[1] L. Wang, M. S. H. Boutilier, P. R. Kidambi, D. Jang, N. G. Hadjiconstantinou, R. Karnik, *Nat. Nanotechnol.* **2017**, *12*, 509.

[2] M. Lozada-Hidalgo, S. Zhang, S. Hu, A. Esfandiar, I. V Grigorieva, A. K. Geim, *Nat. Commun.* **2017**, *8*, 15215.

[3] K. Celebi, J. Buchheim, R. M. Wyss, A. Droudian, P. Gasser, I. Shorubalko, J.-I. Kye, C. Lee, H. G. Park, *Science* **2014**, *344*, 289.

[4] S. P. Koenig, L. Wang, J. Pellegrino, J. S. Bunch, *Nat. Nanotechnol.* **2012**, *7*, 728.

[5] D. Cohen-Tanugi, J. C. Grossman, *Nano Lett.* **2012**, *12*, 3602.

[6] L. Wang, C. M. Williams, M. S. H. Boutilier, P. R. Kidambi, R. Karnik, *Nano Lett.* **2017**, *17*, 3081.

[7] A. T. Kuan, B. Lu, P. Xie, T. Szalay, J. A. Golovchenko, *Appl. Phys. Lett.* **2015**, *106*, 203109.

[8] Y. Zhao, Y. Xie, Z. Liu, X. Wang, Y. Chai, F. Yan, *Small* **2014**, *10*, 4521.

[9] P. R. Kidambi, D. Jang, J.-C. Idrobo, M. S. H. Boutilier, L. Wang, J. Kong, R. Karnik, *Adv. Mater.* **2017**, *29*, 1700277.

[10] G. Wei, X. Quan, S. Chen, H. Yu, *ACS Nano* **2017**, *11*, 1920.

[11] J. S. Bunch, S. S. Verbridge, J. S. Alden, A. M. van der Zande, J. M. Parpia, H. G. Craighead, P. L. McEuen, *Nano Lett.* **2008**, *8*, 2458.

[12] C. Sun, M. S. H. Boutilier, H. Au, P. Poesio, B. Bai, R. Karnik, N. G. Hadjiconstantinou, *Langmuir* **2014**, *30*, 675.

[13] S. C. O'Hern, D. Jang, S. Bose, J. C. Idrobo, Y. Song, T. Laoui, J. Kong, R. Karnik, *Nano Lett.* **2015**, *15*, 3254.

[14] S. C. O'Hern, C. A. Stewart, M. S. H. Boutilier, J. Idrobo, S. Bhaviripudi, S. K. Das, J. Kong, T. Laoui, M. Atieh, R. Karnik, *ACS Nano* **2012**, *6*, 10130.

[15] T. Jain, B. C. Rasera, R. J. S. Guerrero, M. S. H. Boutilier, S. C. O'Hern, J.-C. Idrobo, R. Karnik, *Nat. Nanotechnol.* **2015**, *10*, 1053.

[16] C. J. Russo, J. A. Golovchenko, *Proc. Natl. Acad. Sci. USA* **2012**, *109*, 5953.

[17] R. C. Rollings, A. T. Kuan, J. A. Golovchenko, *Nat. Commun.* **2016**, *7*, 11408.

[18] S. Garaj, W. Hubbard, A. Reina, J. Kong, D. Branton, J. A. Golovchenko, *Nature* **2010**, *467*, 190.

[19] J. Feng, K. Liu, M. Graf, R. D. Bulushev, D. Dumcenco, D. T. L. Alexander, D. Krasnozhon, T. Vuletic, A. Kis, A. Radenovic, *Nano Lett.* **2015**, *15*, 3431.

[20] M. S. H. Boutilier, C. Sun, S. C. O'Hern, H. Au, N. G. Hadjiconstantinou, R. Karnik, *ACS Nano* **2014**, *8*, 841.

[21] P. R. Kidambi, R. A. Terry, L. Wang, M. S. H. Boutilier, D. Jang, J. Kong, R. Karnik, *Nanoscale* **2017**, *9*, 8496.

[22] P. R. Kidambi, D. D. Mariappan, N. T. Dee, A. Vyatskikh, S. Zhang, R. Karnik, A. J. Hart, *ACS Appl. Mater. Interfaces* **2018**, *10*, 10369.

[23] P. R. Kidambi, M. S. H. Boutilier, L. Wang, D. Jang, J. Kim, R. Karnik, *Adv. Matter.* **2017**, *29*, 1605896.

[24] M. S. H. Boutilier, D. Jang, J. C. Idrobo, P. R. Kidambi, N. G. Hadjiconstantinou, R. Karnik, *ACS Nano* **2017**, *11*, 5726.

[25] L. Madauß, J. Schumacher, M. Ghosh, O. Ochedowski, J. Meyer, H. Lebius, B. Ban-d'Etat, M. E. Toimil-Molares, C. Trautmann, R. G. H. Lammertink, M. Ulbricht, M. Schleberger, K. Nordlund, F. Djurabekova, H. A. Wu, A. K. Geim, *Nanoscale* **2017**, *182*, 449.

[26] Y. Qin, Y. Hu, S. Koehler, L. Cai, J. Wen, X. Tan, W. L. Xu, Q. Sheng, X. Hou, J. Xue, M. Yu, D. Weitz, *ACS Appl. Mater. Interfaces* **2017**, *9*, 9239.

[27] A. Zandiatashbar, G.-H. Lee, S. J. An, S. Lee, N. Mathew, M. Terrones, T. Hayashi, C. R. Picu, J. Hone, N. Koratkar, *Nat. Commun.* **2014**, *5*, 3186.

[28] S. P. Surwade, S. N. Smirnov, I. V. Vlassiouk, R. R. Unocic, G. M. Veith, S. Dai, S. M. Mahurin, *Nat. Nanotechnol.* **2015**, *10*, 459.

[29] L. Prozorovska, P. R. Kidambi, *Adv. Matter.* **2018**, 1801179.

[30] T. Kobayashi, M. Bando, N. Kimura, K. Shimizu, K. Kadono, N. Umezu, K. Miyahara, S. Hayazaki, S. Nagai, Y. Mizuguchi, Y. Murakami, D. Hobara, *Appl. Phys. Lett.* **2013**, *102*, 023112.

[31] S. Bae, H. Kim, Y. Lee, X. Xu, J.-S. Park, Y. Zheng, J. Balakrishnan, T. Lei, H. Ri Kim, Y. Il Song, Y.-J. Kim, K. S. Kim, B. Özyilmaz, J.-H. Ahn, B. H. Hong, S. Iijima, *Nat. Nanotechnol.* **2010**, *5*, 574.

[32] M. I. Walker, R. S. Weatherup, N. A. W. Bell, S. Hofmann, U. F. Keyser, *Appl. Phys. Lett.* **2015**, *106*, 023119.

[33] Z. Yuan, J. D. Benck, Y. Eatmon, D. Blankschtein, M. S. Strano, *Nano Lett.* **2018**, *18*, 5057.

[34] D. Jang, J.-C. Idrobo, T. Laoui, R. Karnik, *ACS Nano* **2017**, *11*, 10042.

[35] V. Shvets, *Ph.D. Thesis*, TU Denmark **2017**.

[36] Z. Wang, T. Li, L. Schulte, K. Almdal, S. Ndoni, *ACS Appl. Mater. Interfaces* **2016**, *8*, 8329.

[37] J. Buchheim, R. M. Wyss, I. Shorubalko, H. G. Park, *Nanoscale* **2016**, *8*, 8345.

[38] S. Park, J. M. Yun, U. N. Maiti, H.-S. Moon, H. M. Jin, S. O. Kim, *Nanotechnology* **2014**, *25*, 014008.

[39] X. Bai, X. Zhong, S. Jiang, Y. Huang, X. Duan, *Nat. Nanotechnol.* **2010**, *5*, 190.

[40] S. Huang, M. Dakhchoune, W. Luo, E. Oveisi, G. He, M. Rezaei, J. Zhao, D. T. L. Alexander, A. Züttel, M. S. Strano, K. V. Agrawal, *Nat. Commun.* **2018**, *9*, 2632.

**ADVANCED
SCIENCE NEWS**

www.advancedsciencenews.com

**ADVANCED
MATERIALS**

www.advmat.de

[41] X. Li, W. Cai, J. An, S. Kim, J. Nah, D. Yang, R. Piner, A. Velamakanni, I. Jung, E. Tutuc, S. K. Banerjee, L. Colombo, R. S. Ruoff, *Science* **2009**, *324*, 1312.

[42] M. Hofmann, Y. C. Shin, Y. P. Hsieh, M. S. Dresselhaus, J. Kong, *Nano Res.* **2012**, *5*, 504.

[43] A. W. Tsen, L. Brown, M. P. Levendorf, F. Ghahari, P. Y. Huang, R. W. Havener, C. S. Ruiz-Vargas, D. A. Muller, P. Kim, J. Park, *Science* **2012**, *336*, 1143.

[44] N. Petrone, C. R. Dean, I. Meric, A. M. Van Der Zande, P. Y. Huang, L. Wang, D. Muller, K. L. Shepard, J. Hone, *Nano Lett.* **2012**, *12*, 2751.

[45] P. R. Kidambi, C. Ducati, B. Dlubak, D. Gardiner, R. S. Weatherup, M. B. Martin, P. Seneor, H. Coles, S. Hofmann, *J. Phys. Chem. C* **2012**, *116*, 22492.

[46] P. R. Kidambi, B. C. Bayer, R. Blume, Z.-J. Wang, C. Baehtz, R. S. Weatherup, M.-G. Willinger, R. Schloegl, S. Hofmann, *Nano Lett.* **2013**, *13*, 4769.

[47] P. R. Kidambi, R. Blume, J. Kling, J. B. Wagner, C. Baehtz, R. S. Weatherup, R. Schloegl, B. C. Bayer, S. Hofmann, *Chem. Mater.* **2014**, *26*, 6380.

[48] T. Niu, M. Zhou, J. Zhang, Y. Feng, W. Chen, *J. Am. Chem. Soc.* **2013**, *135*, 8409.

[49] A. C. Ferrari, D. M. Basko, *Nat. Nanotechnol.* **2013**, *8*, 235.

[50] A. Bellunato, H. Arjmandi Tash, Y. Cesa, G. F. Schneider, *ChemPhysChem* **2016**, *17*, 785.

[51] R. Blume, P. R. Kidambi, B. C. Bayer, R. S. Weatherup, Z.-J. Wang, G. Weinberg, M.-G. Willinger, M. Greiner, S. Hofmann, A. Knop-Gericke, R. Schlögl, *Phys. Chem. Chem. Phys.* **2014**, *16*, 25989.

[52] A. I. Altan, J. Chen, *Nanoscale* **2018**, *10*, 11052.

[53] F. Banhart, J. Kotakoski, A. V. Krasheninnikov, *ACS Nano* **2011**, *5*, 26.

[54] L. Wang, X. Zhang, H. L. W. Chan, F. Yan, F. Ding, *J. Am. Chem. Soc.* **2013**, *135*, 4476.

[55] J. H. Lee, E. K. Lee, W. J. Joo, Y. Jang, B. S. Kim, J. Y. Lim, S. H. Choi, S. J. Ahn, J. R. Ahn, M. H. Park, C. W. Yang, B. L. Choi, S. W. Hwang, D. Whang, *Science* **2014**, *344*, 286.

[56] X. Xu, Z. Zhang, J. Dong, D. Yi, J. Niu, M. Wu, L. Lin, R. Yin, M. Li, J. Zhou, S. Wang, J. Sun, X. Duan, P. Gao, Y. Jiang, X. Wu, H. Peng, R. S. Ruoff, Z. Liu, D. Yu, E. Wang, F. Ding, K. Liu, *Sci. Bull.* **2017**, *62*, 1074.

[57] I. V. Vlassiouk, Y. Stehle, P. R. Pudasaini, R. R. Unocic, P. D. Rack, A. P. Baddorf, I. N. Ivanov, N. V. Lavrik, F. List, N. Gupta, K. V. Bets, B. I. Yakobson, S. N. Smirnov, *Nat. Mater.* **2018**, *17*, 318.

[58] R. W. Baker, *Membrane Technology and Applications*, Wiley-Blackwell, Oxford, UK **2012**.

[59] S. Loeb, S. Sourirajan, *Adv. Chem.* **1963**, 117.

[60] J. G. Crespo, K. W. Böddeker, *Membrane Processes in Separation and Purification*, Springer Science & Business Media, Dordrecht, The Netherlands **1994**.

[61] L. M. Robeson, *J. Membr. Sci.* **2008**, *320*, 390.